Influence of Dry-Mixing and Solvent Casting Blending Techniques on the Mechanical and Biological Behavior of Novel Biocompatible Poly(-caprolactone)/Alumina-Toughened

Journal of
*Composites Science*

MDPI

*Article*

# Influence of Dry-Mixing and Solvent Casting Blending Techniques on the Mechanical and Biological Behavior of Novel Biocompatible Poly(ε-caprolactone)/Alumina-Toughened Zirconia Scaffolds Obtained by 3D Printing

**Mattia Di Maro [1,†], Riccardo Pedraza [1,2,3,†], Alessandro Mosca Balma [2], Giovanna Gomez d'Ayala [4], Giovanni Dal Poggetto [4], Giulio Malucelli [5], Ilaria Roato [2], Donatella Duraccio [1,‡], Federico Mussano [2,*,‡] and Maria Giulia Faga [1,‡]**

1 Institute of Sciences and Technologies for Sustainable Energy and Mobility, National Council of Research, Strada delle Cacce 73, 10135 Torino, Italy; mattia.dimaro@stems.cnr.it (M.D.M.); riccardo.pedraza@stems.cnr.it (R.P.); donatella.duraccio@stems.cnr.it (D.D.); mariagiulia.faga@stems.cnr.it (M.G.F.)
2 Department of Surgical Sciences, CIR Dental School, University of Turin, 10126 Turin, Italy; alessandro.moscabalma@unito.it (A.M.B.); ilaria.roato@unito.it (I.R.)
3 Department of Mechanical and Aerospace Engineering, Politecnico di Torino, 10129 Turin, Italy
4 Institute for Polymers, Composites and Biomaterials, National Council of Research, Via Campi Flegrei 34, 80078 Pozzuoli, Italy; giovanna.gomez@ipcb.cnr.it (G.G.d.); giovanni.dalpoggetto@ipcb.cnr.it (G.D.P.)
5 Department of Applied Science and Technology, Local INSTM Unit, Politecnico di Torino, Viale T. Michel 5, 15121 Alessandria, Italy; giulio.malucelli@polito.it
* Correspondence: federico.mussano@unito.it
† These authors contributed equally to this work.
‡ These authors contributed equally to this work.

check for updates

**Citation:** Di Maro, M.; Pedraza, R.; Mosca Balma, A.; Gomez d'Ayala, G.; Poggetto, G.D.; Malucelli, G.; Roato, I.; Duraccio, D.; Mussano, F.; Faga, M.G. Influence of Dry-Mixing and Solvent Casting Blending Techniques on the Mechanical and Biological Behavior of Novel Biocompatible Poly(ε-caprolactone)/Alumina-Toughened Zirconia Scaffolds Obtained by 3D Printing. *J. Compos. Sci.* **2024**, *8*, 194. https://doi.org/10.3390/jcs8060194

Academic Editor: Francesco Tornabene

Received: 29 April 2024
Revised: 9 May 2024
Accepted: 17 May 2024
Published: 21 May 2024



**Abstract:** This work focuses on the study and comparison of two mixing methods for the dispersion of Alumina-Toughened Zirconia (ATZ) within the polymer matrix of Poly(ε-caprolactone) (PCL). The dry-mixing method using solvent-free impact milling (M) and the solvent casting method with chloroform (SC) were investigated. Samples were produced by 3D printing, and specimens were printed at increasing ATZ loadings (namely, 10, 20, and 40 wt.%). The chemico-physical, mechanical, and cell interaction characteristics of the materials prepared with both mixing methods were studied. Solvent mixing allowed better dispersion of the ATZ in the polymer matrix with respect to dry mixing. In addition, dry mixing affected the molecular weight of the PCL/ATZ composites much more than the solvent casting method. For these reasons, materials obtained by solid mixing exhibited the worst mechanical performance with respect to those obtained by solvent casting, which showed increased Young's moduli with increasing ATZ amounts. The in vitro biological response elicited in a mesenchymal stem cell model seemed to be influenced by the mixing method, with a preference for the composites obtained through solvent mixing and containing 20 or 40 wt.% of ATZ.

**Keywords:** Poly(ε-caprolactone); alumina-toughened zirconia; solvent casting; dry mixing; 3D printing

## 1. Introduction

Bone healing capacity, although intrinsically high, can be challenged by non-union fractures, oncologic resections, craniofacial malformations, edentulism, or impaired health conditions (such as diabetes), resulting in large bone defects possibly leading to long-term disability and/or pain [1]. To form new bone tissue in the target area, traumatologists, orthopedists, and oral and maxillofacial surgeons perform bone repair procedures that are estimated to cost, each year, USD 5.5 billion in the US and USD 4.7 billion in Europe [2], while the total cost of bone-repair-related expenditure is estimated to be USD 17 billion per year [3].

These procedures are based on bone grafts harvested from the patient (i.e., autografts), derived from cadavers (allografts), or obtained from other species (xenografts) and artificial scaffolds, i.e., bone graft substitutes [3]. Still regarded by many clinicians as the gold standard, autografts are osteoinductive and osteoconductive, but have limited availability and expose the patient to donor-site morbidity [4,5]. Allografts and xenografts may trigger immune rejection or allow disease transmission, and are less osteoinductive than autografts due to disruptive processing [5]. Favored by the advances in bone tissue engineering, artificial scaffolds [4], albeit very promising, often show low fusion rates due to reduced cell ingrowth and local inflammation upon degradation [5,6].

New biomaterials combining the mechanical features of tailored synthetic polymers with the biocompatible element of inorganic fillers have been proposed, thus minimizing the pitfalls of each component while exploiting their own favorable properties to generate a superior hybrid material. However, for biomedical applications composite technology is mainly used for improving a variety of mechanical, thermal, and biological properties of inert polymers [7–10]. Alumina-Toughened Zirconia (ATZ)-based massive ceramics display the most suitable biological features [11], but are hindered by their mechanical properties, limiting their use in load-bearing applications. Poly(ε-caprolactone) (PCL), a synthetic, biodegradable, aliphatic polyester, is emerging as a promising material among polymers for intra-osseous use, and it has been proposed both in three-dimensional scaffolds [12] and film substrates [13]. Several composite materials were prepared by the sol–gel method, mixing PCL with a series of different fillers like $TiO_2$ [14], CaO [15], $SiO_2$ [16], and $ZrO_2$ [17].

More recently, novel bioactive scaffolds have been synthesized [18], embedding a matrix of PCL–alginate–chitosan with biphasic calcium phosphate (BCP) and zirconia–mullite ($2ZrO_2 \cdot [3Al_2O_3 \cdot 2 \cdot SiO_2]$, with promising mechanical properties and biocompatibility. Yet, the number of components induced a high level of complexity and resulted in a compressive strength of 42.96 ± 1.01 MPa for the best candidate. $ZrO_2$ blended with PCL in silicate cement containing fluorine proved to be biocompatible when implanted in male Wistar rats [19].

Here, three different PCL-ATZ composites varying in their filler content are considered (10, 20, and 40 wt.% ATZ), and were obtained through either solvent casting with $CHCl_3$ or solid mixing with an impact mill and characterized mechanically and in terms of biocompatibility (cell viability). Generally, solvent casting is the most common method used for the preparation of composites to be used for 3D printing [20,21]. This is because solvent mixing offers good dispersion of the filler in the polymer matrix and final powder uniformity for feeding the printer. However, this method can be complex, expensive, and time-consuming and involves the use of solvent that can be dangerous for the environment and human health. The dry-mixing method can overcome these drawbacks, also ensuring a 100% composite yield compared to the solvent-assisted one [22].

## 2. Materials and Methods

### *2.1. Preparation of Materials and Composites*

The powder of ester-terminated polycaprolactone (CAS-n 24980-41-4), used as a polymer matrix (CELLINK PCL TP-60505), with a melting point of 60 °C and relative density of 1.145 g/mL at 25 °C, was purchased from Bico Group (Gothenburg, Sweden). Alumina-Toughened Zirconia (ATZ, made of 20 wt.% $Al_2O_3$ and 80 wt.% 3Y-TZP composed of 3 mol% yttria-stabilized zirconia), used as a filler, was supplied by Tosoh Bioscience (Tokyo, Japan). Chloroform (CAS-n 67-66-3) was purchased from CARLO ERBA Reagents S.r.l. (Cornaredo, Italy). The composites PCL/ATZ were prepared with two different processes: solvent casting with $CHCl_3$ (Table 1) and solid mixing with a homemade impact mill [1]. In both cases, composites at different filler loadings were prepared: neat PCL, PCL/ATZ 90/10, PCL/ATZ 80/20, and PCL/ATZ 60/40. For all composites and in both processes, 3 g of each material was prepared. The solvent casting procedure was carried out by dissolving PCL pellets in chloroform (13.3% *w*/*v*%) under stirring at RT for 24 h. After that, ATZ was added to the solution, which was left under stirring for 6 h. Then, the mixture was put

under a hood and poured into Petri dishes, and we waited for the complete evaporation of the chloroform. To ease the detachment of the composites after $CHCl_3$ evaporation, aluminum foil was used to cover the Petri dishes. The resulting material was cut into small pieces to be used with the 3D printer. The solid-mixing process (Table 2) was carried out in dry conditions using the mentioned homemade impact mill. PCL powders were mixed with ATZ at 8000 rpm for 30 s. The as-obtained powders were used for the 3D printing step. PCL powder was also subjected to the same processes and used as a control material.

**Table 1.** Composition of formulations utilized for solvent casting method.

| | PCL | PCL/ATZ 90/10 | PCL/ATZ 80/20 | PCL/ATZ 60/40 |
|---|---|---|---|---|
| PCL (g) | 3 | 2.7 | 2.4 | 1.8 |
| ATZ (g) | / | 0.3 | 0.6 | 1.2 |
| $CHCl_3$ (mL) | 22.55 | 22.55 | 22.55 | 22.55 |

**Table 2.** Composition of formulations utilized for solid-mixing method.

| | PCL | PCL/ATZ 90/10 | PCL/ATZ 80/20 | PCL/ATZ 60/40 |
|---|---|---|---|---|
| PCL (g) | 3 | 2.7 | 2.4 | 1.8 |
| ATZ (g) | / | 0.3 | 0.6 | 1.2 |

### *2.2. Sample Printing*

Three-dimensional scaffolds were printed using a thermoplastic pneumatic printhead with a BIO X 3D bioprinter from CELLINK. STL, and, consequently, gcode files were designed with a rectilinear geometry to mimic bone's trabecular structure. Three-dimensional files were designed with the SolidWorks program (Dassault Systèmes—SolidWorks Corporation, Vélizy-Villacoublay, France), and subsequent slicing was performed with the Repetier-Host program (Hot-World GmbH & Co. KG, Knickelsdorf, Germany). For cell adhesion and cell spreading tests, samples were designed as disks with a 10 mm diameter, a 1 mm thickness, and an infill percentage of 100%. The samples for SEM analysis were designed with a 6 mm diameter, a 1.5 mm thickness, and a 40% infill percentage. Scaffolds were produced as disks with a 10 mm diameter and a 1.35 mm thickness. The infill percentage was 40% and the printbed temperature was set at 25 °C with a clean chamber fan on. Printhead temperature was different from sample to sample, namely, 110 °C for neat PCL, 120 °C for PCL/ATZ 90/10, 125 °C for PCL/ATZ 80/20, and 145 °C for PCL/ATZ 60/40. A nozzle of 0.4 mm in diameter was employed; the imposed pressure was 190 kPa and the printing speed was set at 1 mm/s.

### *2.3. X-ray Diffraction (XRD)*

An evaluation of the effect of the processing technique on the structure of neat PCL was performed by wide-angle X-ray powder diffraction (WAXD). WAXD experiments were carried out by using a PANalytical PW3040/60 X'Pert PRO MPD diffractometer, working at 45 kV and 40 mA, and using Bragg–Brentano geometry (source: high-power ceramic tube PW3373/10 LFF with Cu anode). WAXD profiles were obtained using Ni-filtered Cu Kα radiation (λ = 0.15418 nm) with a continuous scan rate of 0.04°/s (scan step size: 0.0167°; time per step: 53 s) in the 5–70° range. The crystallinity degree of PCL ($\chi_c$) was calculated as the ratio between the intensity of the crystalline phase and the total diffraction intensity. The polymer crystalline phase intensity was calculated by subtracting the amorphous contribution from the total intensity of the diffraction spectrum. The contribution of the amorphous fraction of PCL was estimated by building a Gaussian-shaped baseline subtended to the XRD spectrum using Origin Lab 8.5 software.

### *2.4. Gel Permeation Chromatography (GPC)*

The average molecular weight of PCL-based samples was determined through Gel Permeation Chromatography (GPC) analysis, using a GPC Max Viscotek equipped with a

Malvern TDA 305 comprising refractive index (RI), right-angle laser-light scattering (RALS), low-angle laser-light scattering (LALS), and intrinsic viscosity (IV) detectors.

Sections of PCL scaffolds were cut and solubilized in chloroform at a concentration of around 5 mg/mL and filtered using a 0.22 µm PTFE filter. A volume of 100 µL was injected and eluted in $CHCl_3$ (Romil) at a flux of 0.8 mL/min through a column set composed of a precolumn and two Phenogel Phenomenex columns, with exclusion limits of $10^6$ and $10^3$ Da. All samples were evaluated with universal calibration (polystyrene standards ranging between 560 and 2.45 kDa).

### *2.5. Scanning Electron Microscopy (SEM)*

Micrographs of the sample surfaces and cross-section morphology were acquired using scanning electron microscopy (SEM, ZEISS EVO 50 XVP—Oberkochen, Germany—with LaB6 source) to study the surface morphology of all composite materials. To allow for sample observations and avoid any charge effect, samples were metalized with a 10 nm coating of gold before the analysis. To observe the cross-section, samples were frozen in liquid nitrogen to induce a brittle fracture.

### *2.6. Mechanical Properties*

Tensile tests were carried out with an Instron 5966 dynamometer (Norwood, MA, USA). The tests were conducted at room temperature on specimens measuring $50 \times 3 \times 1$ mm$^3$. The elongation zone was defined by placing the clamps at 2 cm intervals. The methodology used was as follows: 1 mm/min speed until 0.2% deformation, and then 20 mm/min until breakage. The data measured by this test were Young's modulus (E), elongation at break (%), and tensile strength (MPa). Mechanical data were averaged over five separate tests for each group of samples.

Hardness (Shore D scale) was evaluated using a Classic Durometer (Sauter model). Five repetitions were carried out for each group of samples on specimens measuring $8 \times 8 \times 1$ mm$^3$.

### *2.7. Surface Roughness*

The surface roughness was evaluated using a contact profilometer (Form Talysurf 120) equipped with a 2 µm diamond conical stylus. $S_a$, $S_{sk}$, and $S_{ku}$ parameters were measured, keeping the area of the measurement at 2 mm × 1 mm and using a cut-off of 0.8 mm.

### *2.8. Cell Viability*

To assess the biological compatibility of the composites, a widely used mesenchymal stem cell model was adopted [9,23]. ASC52hTert (ATCC) adipose stem cells were cultured in Alpha-MEM (Life Technologies, Milano, Italy) supplemented with 10% FBS, 100 U/mL penicillin, and 100 µg/mL streptomycin. Sub-confluent cultures were maintained to avoid contact inhibition, and the cells were incubated in a humidified atmosphere containing 5% $CO_2$ at 37 °C.

For cell viability, 3D scaffolds were positioned in 48-well culture dishes (Euroclone S.p.A., Milano, Italy); then, 25000 ASC52hTert cells were seeded on each scaffold and kept under incubation in Alpha-MEM growth medium (Sigma-Aldrich, Milano, Italy). Viability tests were performed on all the compositions (on at least three different specimens). After 3, 7, and 14 days, viability was assessed using a Cell Titer GLO kit (Promega, Madison, WI, USA) following the manufacturer's instructions and analyzed with a luminometer (LuMate 4400, Awareness Technology, Wiener Neudorf, Austria).

### *2.9. Statistical Analyses*

The evaluation of statistical differences was conducted using STATA software (version 18.0; StataCorp, College Station, TX, USA). One-way ANOVA was performed to evaluate differences in group variances at different time steps. A *T*-test was performed to assess statistically significant differences between groups. $p < 0.05$ was considered statistically significant.

## 3. Results

### 3.1. Structural Analysis

Figure 1 shows the WAXD spectra of neat PCL, before and after the printing process performed after both the solvent casting (1A) and the milling process (1B). Neat PCL shows a typical polymer diffraction profile characterized by three sharp crystalline peaks at 2θ of 21.7°, 22.3°, and 24.0°, respectively, related to the (110), (111), and (200) planes of the orthorhombic PCL crystals. Also, a halo below the crystalline peaks, related to the scattering of the PCL amorphous phase, is visible [24]. Polymer processing does not modify the crystalline structure of PCL, which retains its orthorhombic structure both when subjected to solvent casting and when ground during impact milling. It is interesting to observe that the PCL obtained following chloroform evaporation (red curve, Figure 1A) shows an increase in the width of the crystalline peaks (110) and (200), while the peak related to the (111) plane is absent. As reported for similar systems [25], this behavior can be attributed to the presence of the solvent during crystallization, which could remain entrapped among the molecular chains of the polymer and lead to the formation of crystals larger in size than those of the commercial PCL. After the 3D printing process, the peak related to the (111) plane appears again (Figure 1A—blue curve): the melting process during 3D printing allows for the complete evaporation of the remaining solvent, and the structure is similar to that of the unprocessed powder. Unlike solvent casting, the dry-mixing process does not involve changes in the crystalline structure (i.e., the black and red curves of Figure 1B overlap), and the 3D-printed PCL shows crystalline peaks in the same position and of the same width as those observed for the unprocessed material. Finally, for both the solvent casting and impact milling of 3D-printed PCL, a change in the relative intensities of the three crystalline peaks is observed, indicating that the 3D printing process gives rise to a different crystalline orientation of PCL. The crystallinity degree ($\chi_c$) of neat PCL and its composites was measured based on the WAXD profiles and reported in Table 3. Commercial PCL powder shows a crystallinity degree of 52%. After solvent casting, the crystallinity degree of PCL decreases to 45% due to the above-mentioned solvent effect on crystallization during solvent evaporation. After the 3D printing the crystallinity degree of PCL increases again up to 50%. No difference is observed in the crystallinity degree of PCL powder and the material after impact milling (i.e., both materials show a crystallinity degree of 52%).

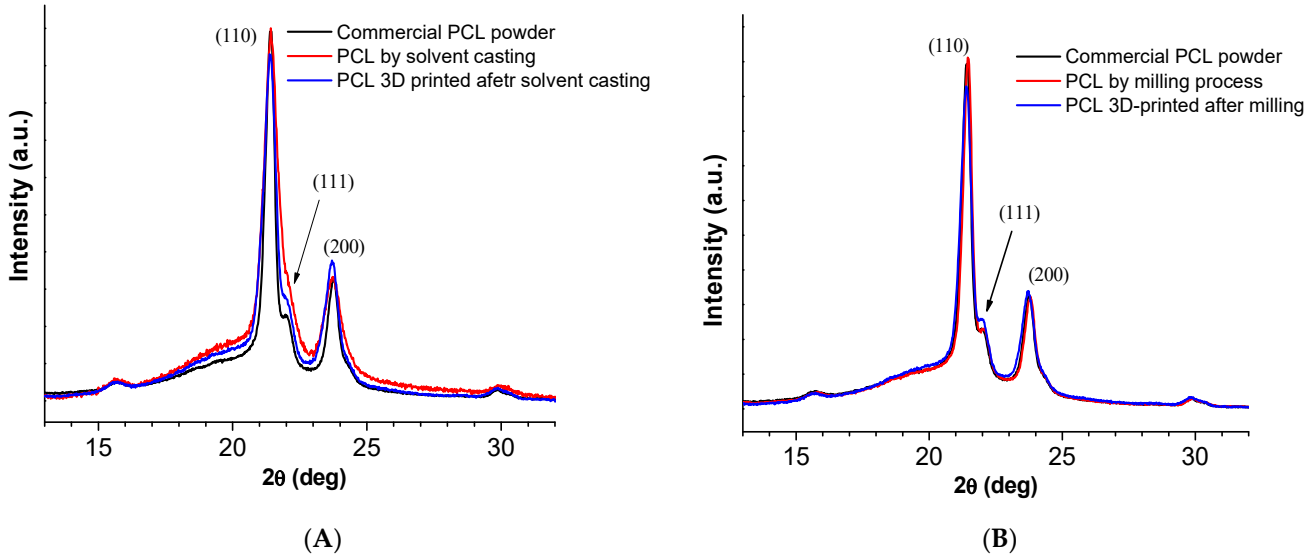


**Figure 1.** WAXD patterns of 3D-printed PCL after solvent casting (**A**) and dry-mixing (**B**) processes.

**Table 3.** Weight-average molecular weight ($M_w$), number-average molecular weight ($M_n$), and intrinsic viscosity (IV) of neat PCL and its composites with ATZ, obtained by solvent casting (SC) and milling (M).

| Sample | $x_c$ (%) | $M_w$ (Da) | $M_n$ (Da) | IV (dL/g) |
|---|---|---|---|---|
| PCL | 52 ± 1 | 97,411 | 55,172 | 1.135 |
| PCL_3D SC | 50 ± 1 | 65,251 | 37,449 | 1.092 |
| PCL_3D M | 49 ± 2 | 61,757 | 32,876 | 1.068 |
| PCL/ATZ 90/10 SC | 54 ± 1 | 68,895 | 51,668 | 1.094 |
| PCL/ATZ 80/20 SC | 54 ± 1 | 59,614 | 39,653 | 0.936 |
| PCL/ATZ 60/40 SC | 54 ± 1 | 49,227 | 27,322 | 0.649 |
| PCL/ATZ 90/10 M | 53 ± 2 | 53,169 | 44,876 | 0.991 |
| PCL/ATZ 80/20 M | 53 ± 1 | 46,690 | 39,111 | 0.829 |
| PCL/ATZ 60/40 M | 52 ± 2 | 31,073 | 23,041 | 0.637 |

A slight increase in crystallinity degree is observed for the composites with respect to neat PCL. The materials printed by solvent casting show a $\chi_c$ of 54% independently of the ATZ amount. Similarly, composites printed by dry mixing exhibit a crystallinity of 52–53%. This work agrees with the literature, where it is reported that ATZ acts as a heterogeneous nucleating agent when added to a polymer matrix, increasing its crystallinity [26]. However, as also found for other fillers, the crystallinity remains almost constant as the amount of ATZ increases [27].

### *3.2. GPC*

GPC analyses were performed to evaluate any changes in PCL's molecular weight after 3D printing. The weight-average molecular weight ($M_w$), number-average molecular weight ($M_n$), and intrinsic viscosity (IV) of PCL-based composites obtained from both the solution and solid mixing were determined; they are listed in Table 3.

The comparison between the $M_w$ and $M_n$ of PCL and PCL_3D highlighted that the 3D printing process induced the partial degradation of PCL. As regards the composites obtained through solution mixing, a gradual decrease in molecular weights and intrinsic viscosity was observed with increasing ATZ loading. Surprisingly, in the presence of 10 wt.% ATZ, $M_w$ appeared comparable to that of PCL_3D, whereas $M_n$ was significantly higher. At this concentration, ATZ is probably able to thermally stabilize PCL during the 3D printing process, as already reported in the literature [28,29].

When the concentration of the inorganic filler approached 20 wt.%, there was no appreciable variation in $M_w$ and $M_n$, while an increase to 40 wt.% accounted for a significant reduction in both molecular weights compared to PCL_3D.

A similar trend was observed in the case of solid mixed composites. $M_w$, $M_n$, and IV gradually decreased with increasing ATZ loading, and the presence of 10 wt.% ATZ reduced the degrading effect of the 3D printing process, reflected as an $M_n$ higher than that of PCL-3D.

The comparison between the molecular weights of the two types of composites (obtained from the solution and solid mixing) highlighted that the mixing process in the mill had a further degrading effect on PCL. Indeed, the $M_w$ and $M_n$ of the milling composites were lower with respect to their counterparts obtained from solvent casting.

### *3.3. Morphological Analysis (SEM)*

According to the images produced using secondary electrons (Figure 2), the filler was dispersed in a mainly homogeneous way on the polymer surface of the 3D-printed material obtained from solvent casting (A, B, C). The composites obtained through dry mixing (D, E, F) show worse dispersion of the ATZ powder on the scaffold surface. The incomplete dispersion of the filler is evidenced by the major presence of filler agglomerates (red circle in Figure 2D). It is also interesting to note how the agglomerates increase in

number and size as the filler concentration increases. Also, the presence of voids is evident in the composites obtained by the dry-mixing procedure.

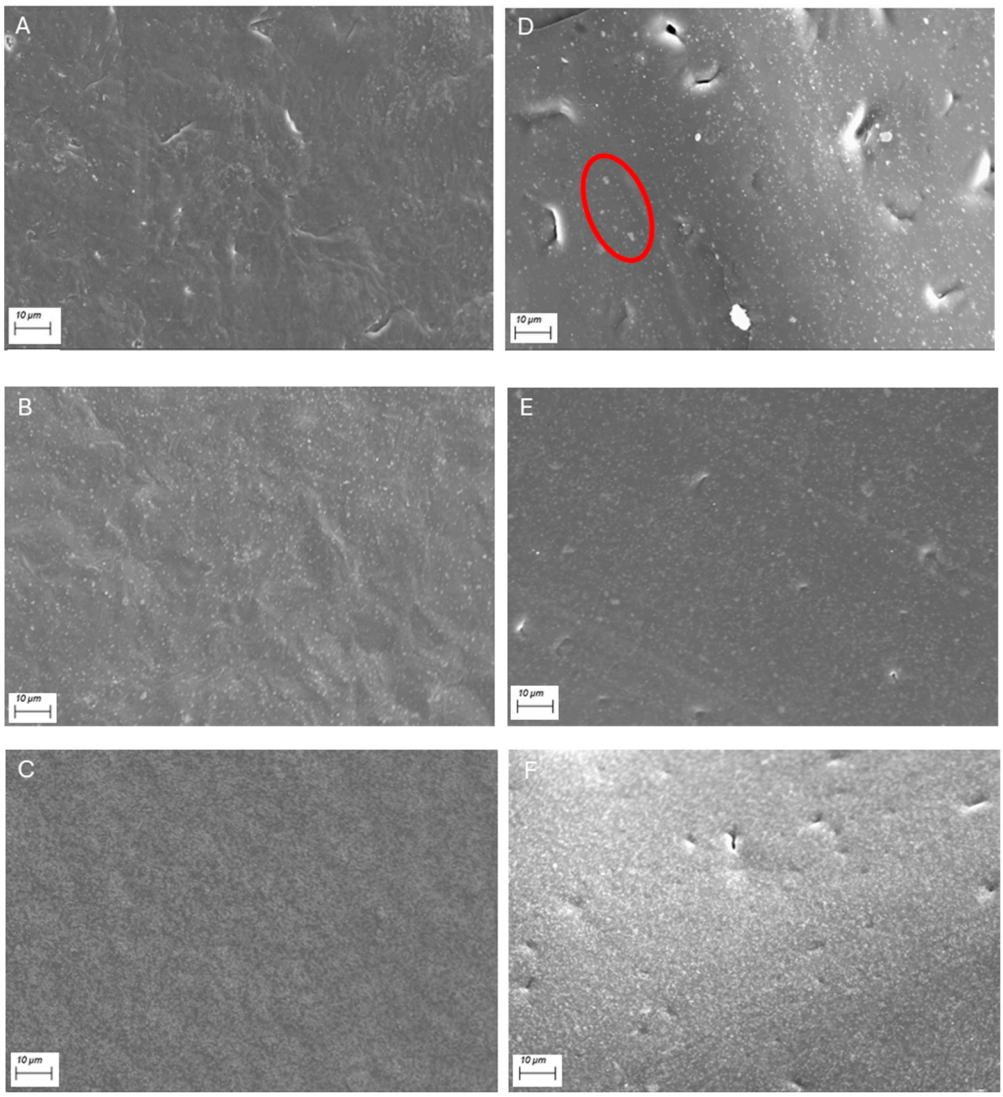


**Figure 2.** Scanning electron micrographs of PCL composite surfaces: (**A**) 3D-printed PCL/ATZ 90/10 SC (**A**), (**B**) PCL/ATZ 80/20 SC, and (**C**) PCL/ATZ 60/40 SC; (**D**) 3D-printed PCL/ATZ 90/10 M, (**E**) PCL/ATZ 80/20, and (**F**) PCL/ATZ 60/40 M (the red circle, in D, indicates a particularly relevant agglomeration of ATZ).

The fracture surfaces of the composites confirm the dispersion of ATZ already observed in Figure 2. For the sake of brevity, only the SEM images of 3D-printed PCL/ATZ 90/10 obtained by solvent casting and milling are reported in Figure 3A and Figure 3B, respectively. The images clearly indicate that the solvent casting method allows to obtain a better dispersion and better distribution of the filler into the polymer matrix with respect to that found when solid mixing is used. Agglomerations of ATZ (highlighted in blue) are evident. Also, ATZ particles appear detached from the matrix, as indicated by the presence of voids (white arrows) in Figure 3B, suggesting a weak filler–polymer interface. This is due to the poor affinity among the ceramic filler and the polymer, as also demonstrated for other composites [26,30].

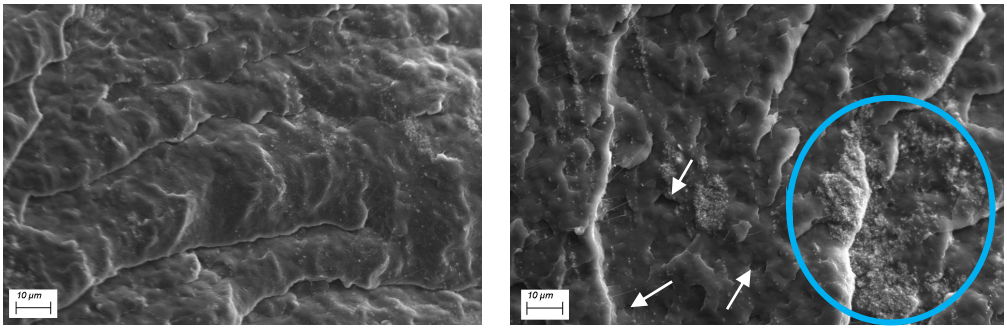


(**A**) (**B**)

**Figure 3.** Scanning electron micrographs of the fractured surface of PCL/ATZ 90/10 obtained by solvent casting (**A**) and dry mixing (**B**) (white arrows indicate the presence of voids, while the highlighted blue area points out a remarkable agglomeration of ATZ).

### *3.4. Mechanical Properties*

The mechanical properties of 3D-printed PCL and its composites with ATZ were evaluated by stress–strain tests. The values of Young's modulus (*E*), elongation at break ($\varepsilon_b$), tensile strength ($\sigma_b$), and hardness (shore D) are presented in Table 4. The corresponding stress–strain curves are shown in Figure 4.

**Table 4.** Mechanical parameters (from tensile tests) measured for PCL and its composites printed from both solvent and dry-mixing materials.

| Sample | E (MPa) | $\varepsilon_b$ (%) | $\sigma_b$ (MPa) | Shore D |
|---|---|---|---|---|
| PCL blank 3D-printed | 516 ± 37 | 581 ± 42 | 20.8 ± 2.7 | 56.2 ± 1.3 |
| PCL/ATZ 90/10 SC | 630 ± 64 | 533 ± 43 | 21.6 ± 2.1 | 57.3 ± 2.1 |
| PCL/ATZ 80/20 SC | 810 ± 90 | 324 ± 26 | 15.2 ± 0.6 | 62.8 ± 2.5 |
| PCL/ATZ 60/40 SC | 943 ± 205 | 4.7 ± 0.7 | 9.1 ± 0.8 | 65.1 ± 3.1 |
| PCL/ATZ 90/10 M | 521 ± 134 | 430 ± 36 | 22.1 ± 2.8 | 56.1 ± 2.8 |
| PCL/ATZ 80/20 M | 543 ± 277 | 348 ± 41 | 17.2 ± 1.1 | 65.5 ± 1.1 |
| PCL/ATZ 60/40 M | 246 ± 138 | 9.54 ± 4.46 | 10.2 ± 0.6 | 65.7 ± 4.5 |

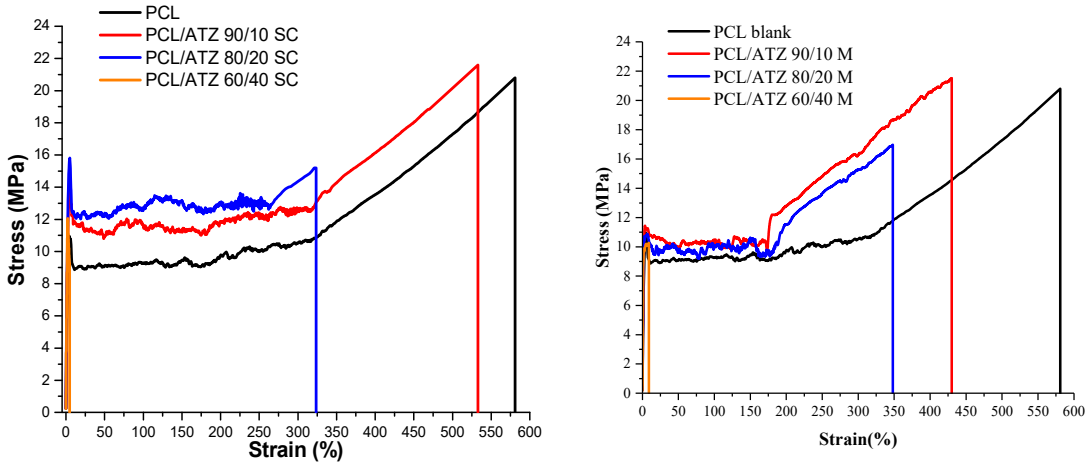


(**A**) (**B**)

**Figure 4.** Stress–strain curves of 3D-printed PCL and its composites, obtained by solvent casting (**A**) and dry-mixing (**B**) processing techniques.

Confirming the reinforcing effect already observed for ATZ [26], the composites prepared from the material mixed by solvent casting show a Young's modulus that increases

as the concentration of the ATZ filler increases (Table 4). In particular, the Young's modulus ($E$) increases from 516 ± 37 MPa, observed for neat PCL, to 810 ± 90 MPa when 20 wt% of ATZ is added to the polymer, up to 943 ± 205 MPa when the amount of ATZ in the composite is 40 wt%. However, ductility and tensile strength decrease with increasing ATZ loading. It is observed that $\varepsilon_b$ decreases as the filler concentration increases, from 581% (for the neat polymer) to 324%, when 20 wt.% filler is incorporated into the polymer, while it drops drastically to 5% when the concentration is 40 wt.%. Finally, the addition of ATZ leads to a slight but gradual increase in the hardness of the materials, which goes from 56.2, observed for neat PCL, to 65.1 observed for PCL ATZ 60/40 SC. The 3D-printed composites obtained by dry mixing show different mechanical behavior. In fact, a general decrease in mechanical properties is observed as the amount of ATZ added to the polymer increases. Although PCL/ATZ 90/10 M shows mechanical properties comparable to neat PCL, significant worsening of $E$ and $\varepsilon_b$ is observed for both PCL/ATZ 80/20 M and PCL/ATZ 60/40 M. In particular, the Young's modulus observed for PCL/ATZ 60/40 M is even lower than that of PCL/ATZ 80/20 M (i.e., 246 ± 138 MPa vs. 80/20 543 ± 277 MPa). This behavior can be explained by considering the detrimental effect induced by the presence of aggregates (and voids) and by the decrease in PCL's molecular weight, observed by GPC analysis. As already discussed, the solid-mixing process could induce degradation of the polymer chains, which increases with increasing the filler loading. This results in a reduction in the mechanical parameters [31].

### 3.5. Surface Roughness

Surface roughness measurements were performed to assess the surface morphology of different compositions and to evaluate the possible influence of the mixing process on the selected surface parameters: arithmetical mean height ($S_a$), Skewness ($S_{sk}$), and Kurtosis ($S_{ku}$). The results are listed in Table 5 [32].

**Table 5.** Arithmetical mean height ($S_a$), Skewness ($S_{sk}$), and Kurtosis ($S_{ku}$) of PCL and its composites.

| Sample | $S_a$ (μm) | $S_{sk}$ | $S_{ku}$ |
|---|---|---|---|
| Neat PCL | 6.461 | −0.0823 | 2.841 |
| PCL/ATZ 90/10 SC | 9.175 | 0.06053 | 2.707 |
| PCL/ATZ 80/20 SC | 7.484 | 0.504 | 3.035 |
| PCL/ATZ 60/40 SC | 11.03 | 0.3712 | 2.716 |
| PCL/ATZ 90/10 M | 15.73 | −0.2934 | 2.751 |
| PCL/ATZ 80/20 M | 11.63 | −0.02216 | 2.503 |
| PCL/ATZ 60/40 M | 10.71 | −0.1473 | 2.601 |

All the samples differ from each other significantly in what concerns the $S_a$ parameter; additionally, it is worth noticing that for both the SC and M samples, the increase in the amount of filler from 10 to 20 wt.% caused a significant reduction in this parameter. Only for PCL/ATZ 60/40 the $S_a$ parameters are similar for both the M and SC methods.

An important difference between SC and M is in the $S_{sk}$ values, which were all positive for the SC samples and negative for the M samples. In particular, the negative $S_{sk}$ values exhibited by the M samples were due to the high number of negative peaks, which appeared as pits on the surface (Figure 2).

### 3.6. Cell Viability

The data obtained from viability tests conducted for 3, 7, and 14 days showed a predictable increase in RLU values, suggesting cell proliferation (Figure 5). On day 3, the ASCs grew similarly in all conditions without achieving any statistically significant difference among the investigated samples. It may be noted only that the values of the SC samples were slightly higher than the milled ones ($p$ = 0.018). This pattern did not seem to be altered on day 7, except for PCL/ATZ 90/10 SC, which was higher than its milled counterpart (PCL/ATZ 90/10 M) in a statistically significant way ($p << 0.01$).

Conversely, during the third time step, there was an appreciable difference between the SC and M specimens regarding PCL/ATZ 80/20 and PCL/ATZ 60/40, which both displayed statistically significantly higher values when obtained through solvent casting than through milling ($p = 0.003$ and $p = 0.001$, respectively). Hence, it may be concluded that SC allowed for a higher proliferation rate compared to the milling process.

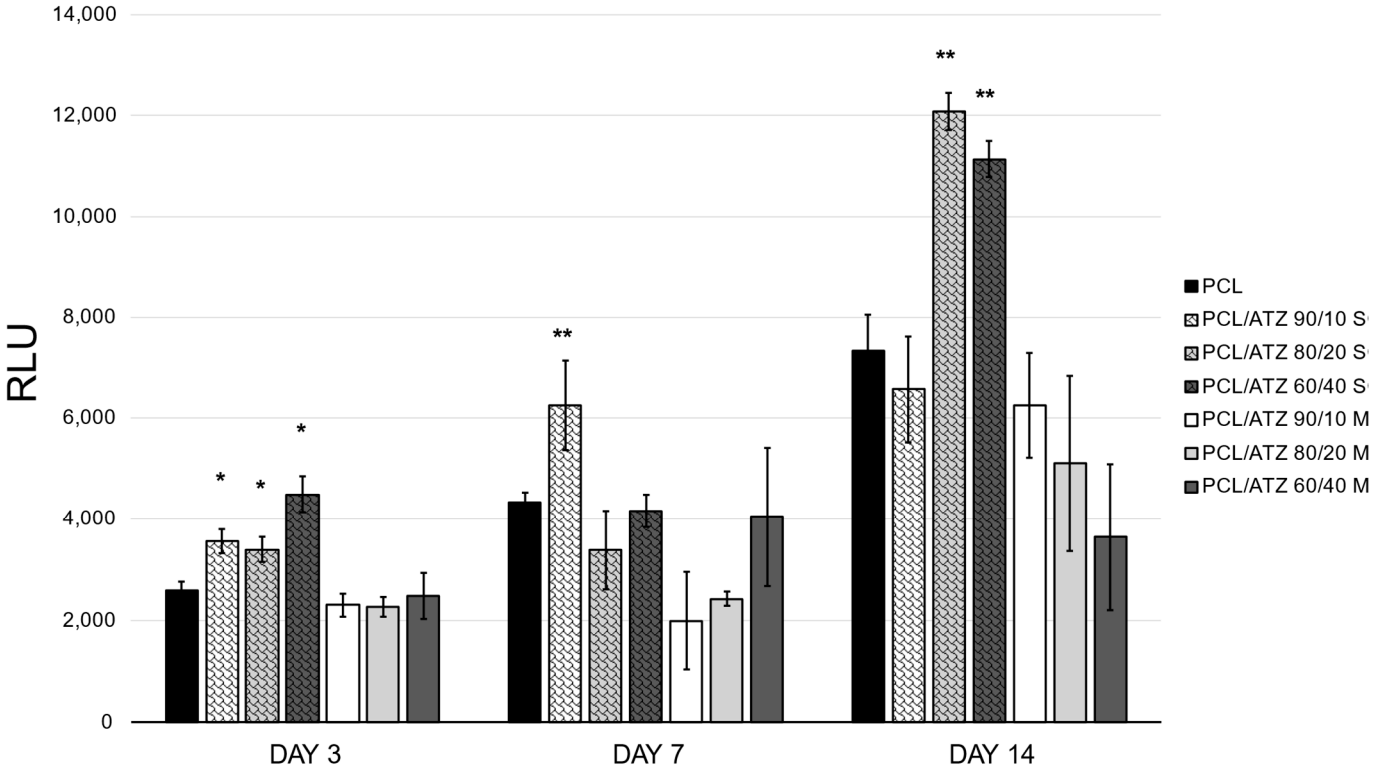


**Figure 5.** Relative Light Unit (RLU), related to the number of live cells, of each sample divided by time step ((*) for $p < 0.05$ and (**) for $p < 0.01$).

## 4. Discussion

This work aimed to prepare novel 3D-printed biocompatible scaffolds based on PCL, a synthetic polymer widely exploited in the biomedical field [33] reinforced with Alumina-Toughened Zirconia (ATZ). PCL-ATZ composites were prepared at different ATZ loadings (10, 20, and 40 wt.%) and by using two different mixing techniques. The idea was to compare the effect of dry mixing (i.e., without solvent) with the traditionally most used solvent mixing method. Three-dimensionally-printed materials were characterized in terms of their mechanical and biological response.

WAXD and GPC analyses were carried out to evaluate how the mixing process affects the crystalline structure and molecular weight of PCL, both before and after the 3D printing process. The crystallinity degree of neat PCL obtained by 3D printing is slightly lower than that of PCL pellets. However, no substantial difference is observed in the crystallinity degree between the PCL printed from solvent mixing and that printed from impact milling (i.e., both the obtained materials show a crystallinity of 50%). Similarly, the molecular weight of neat PCL after 3D printing is lower than that of unprocessed PCL. Moreover, it is observed that the dry mixing leads to a more accentuated decrease in the molecular weight of PCL compared to that from solution; the greater the amount of ATZ in the material, the greater the decrease. Since no decrease in molecular weight is observed for neat PCL printed after milling, it is reasonable to assume that the molecular weight of the polymer decreases because of the degradation processes activated by dry mixing and catalyzed by the presence of ATZ [34,35]. In general, increasing the filler loading results in a decrease in the distance

between the filler particles, leading to their agglomeration and a reduction in the interfacial area between the matrix and filler. This causes a decrease in the thermal stability of the polymer matrix , which becomes more easily degradable [36]. This effect turns out to be remarkable during dry mixing, where contact between the polymer matrix and filler was caused by collision. The polymer degradation induced by dry mixing can account for the worse observed mechanical properties.

From the morphological analysis of the composites, it emerges that the distribution of the filler in the polymer is more homogeneous for solvent-mixed materials. Indeed, dry-mixed material shows a greater presence of aggregates, even at low filler concentrations. Solid mixing, although advantageous from a cost perspective given the absence of solvent and the shorter time required for the mixing process, do not always allow to obtain a good dispersion of the filler in the polymer matrix, as also reported in the literature [10,37]. The dispersion of filler together with the molecular weight of the polymer matrix influence the mechanical properties; indeed, the materials mixed by impact milling show worse mechanical behavior. The poor filler dispersion can also explain the $S_{sk}$ value; indeed, the presence of pits found in the M samples could result from the higher quantities of filler aggregates that lead to the formation of weak interfaces, also occurring after the printing process.

The cell viability analysis carried out on the samples mixed by solvent casting shows an increase in the rate of cell proliferation for each material, with a particularly encouraging result for PCL/ATZ 80/20 SC, whose RLU after 14 days is significantly higher than that of PCL/ATZ 60/40 SC. Conversely, the cell proliferation in the samples prepared by dry mixing up to day 7 shows an increase directly proportional to the filler loading, while on day 14, a lower RLU is found for those samples with a higher ATZ content (i.e., the RLU after 14 days of PCL/ATZ 60/40 M is lower than that observed for PCL/ATZ 80/20 M, which, in turn, is lower than that recorded for PCL/ATZ 90/10 M). This finding highlightes that materials prepared by dry mixing have poorer interaction with the cellular material than those mixed in chloroform and also than neat PCL.

## 5. Conclusions

Finding alternative ways to process materials in an efficient and eco-friendly manner has always been an interesting challenge. In this work, we have compared two types of mixing techniques, solvent casting and impact milling (solvent-free), to find out whether it is possible to obtain similar or improved mechanical and biological properties in different types of composites obtained by adding a ceramic filler (ATZ) inside a polymeric matrix (PCL). Solvent casting allowed to obtain 3D-printed scaffolds with superior mechanical properties compared to those shown by materials derived from dry mixing. The increase in the concentration of ATZ, coupled with milling, led to a detrimental effect on the polymer's molecular weight, its mechanical performance, and even its biological properties. Overall, PCL/ATZ 80/20 SC showed the highest cell proliferation rate and good mechanical properties (lower than PCL/ATZ 60/40 SC, but still better than all the others). Future studies may conveniently exhaustively explore the biological response elicited by 3D-printed samples obtained through this mixing technique.

**Author Contributions:** Conceptualization, A.M.B. and R.P.; methodology, A.M.B. and R.P.; validation, A.M.B., R.P. and M.D.M.; formal analysis, all authors; investigation, all authors; resources, F.M., M.G.F. and D.D.; data curation, A.M.B., R.P. and M.D.M.; writing—original draft preparation, all authors; writing—review and editing, all authors; visualization, F.M., M.G.F. and D.D.; supervision, F.M., M.G.F. and D.D.; project administration, F.M., M.G.F. and D.D. All authors have read and agreed to the published version of the manuscript.

**Funding:** This research was funded by Ministero dell'Università e della Ricerca (MIUR) grant number PRIN 2020 Concerto 2020BN5ZW9. And the APC was funded by University of Turin.

**Data Availability Statement:** The original contributions presented in this study are included in the article. Further inquiries can be directed to the corresponding author.

**Conflicts of Interest:** The authors declare no conflicts of interest.

## References


1. Sallent, I.; Capella-Monsonís, H.; Procter, P.; Bozo, I.Y.; Deev, R.V.; Zubov, D.; Vasyliev, R.; Perale, G.; Pertici, G.; Baker, J. The few who made it: Commercially and clinically successful innovative bone grafts. *Front. Bioeng. Biotechnol.* **2020**, *8*, 952. [CrossRef]
2. Amini, A.R.; Laurencin, C.T.; Nukavarapu, S.P. Bone tissue engineering: Recent advances and challenges. *Crit. Rev. Biomed. Eng.* **2012**, *40*, 363–408. [CrossRef] [PubMed]
3. Ho-Shui-Ling, A.; Bolander, J.; Rustom, L.E.; Johnson, A.W.; Luyten, F.P.; Picart, C. Bone regeneration strategies: Engineered scaffolds, bioactive molecules and stem cells current stage and future perspectives. *Biomaterials* **2018**, *180*, 143–162. [CrossRef] [PubMed]
4. Morris, M.T.; Tarpada, S.P.; Cho, W. Bone graft materials for posterolateral fusion made simple: A systematic review. *Eur. Spine J.* **2018**, *27*, 1856–1867. [CrossRef] [PubMed]
5. Haugen, H.J.; Lyngstadaas, S.P.; Rossi, F.; Perale, G. Bone grafts: Which is the ideal biomaterial? *J. Clin. Periodontol.* **2019**, *46*, 92–102. [CrossRef] [PubMed]
6. Buser, Z.; Brodke, D.S.; Youssef, J.A.; Meisel, H.-J.; Myhre, S.L.; Hashimoto, R.; Park, J.-B.; Yoon, S.T.; Wang, J.C. Synthetic bone graft versus autograft or allograft for spinal fusion: A systematic review. *J. Neurosurg. Spine* **2016**, *25*, 509–516. [CrossRef] [PubMed]
7. Corcione, C.E.; Gervaso, F.; Scalera, F.; Padmanabhan, S.K.; Madaghiele, M.; Montagna, F.; Sannino, A.; Licciulli, A.; Maffezzoli, A. Highly loaded hydroxyapatite microsphere/PLA porous scaffolds obtained by fused deposition modelling. *Ceram. Int.* **2019**, *45*, 2803–2810. [CrossRef]
8. Wang, C.; Meng, C.; Zhang, Z.; Zhu, Q. 3D printing of polycaprolactone/bioactive glass composite scaffolds for in situ bone repair. *Ceram. Int.* **2022**, *48*, 7491–7499. [CrossRef]
9. Roato, I.; Genova, T.; Duraccio, D.; Ruffinatti, F.A.; Zanin Venturini, D.; Di Maro, M.; Mosca Balma, A.; Pedraza, R.; Petrillo, S.; Chinigò, G. Mechanical and Biological Characterization of PMMA/$Al_2O_3$ Composites for Dental Implant Abutments. *Polymers* **2023**, *15*, 3186. [CrossRef]
10. Duraccio, D.; Strongone, V.; Faga, M.; Auriemma, F.; Mussano, F.; Genova, T.; Malucelli, G. The role of different dry-mixing techniques on the mechanical and biological behavior of UHMWPE/alumina-zirconia composites for biomedical applications. *Eur. Polym. J.* **2019**, *120*, 109274. [CrossRef]
11. Schierano, G.; Mussano, F.; Faga, M.G.; Menicucci, G.; Manzella, C.; Sabione, C.; Genova, T.; Degerfeld, M.M.v.; Peirone, B.; Cassenti, A. An alumina toughened zirconia composite for dental implant application: In vivo animal results. *BioMed Res. Int.* **2015**, *2015*, 157360. [CrossRef] [PubMed]
12. Hutmacher, D.W.; Schantz, T.; Zein, I.; Ng, K.W.; Teoh, S.H.; Tan, K.C. Mechanical properties and cell cultural response of polycaprolactone scaffolds designed and fabricated via fused deposition modeling. *J. Biomed. Mater. Res. Off. J. Soc. Biomater. Jpn. Soc. Biomater. Aust. Soc. Biomater. Korean Soc. Biomater.* **2001**, *55*, 203–216. [CrossRef]
13. Khor, H.L.; Ng, K.W.; Schantz, J.-T.; Phan, T.-T.; Lim, T.C.; Teoh, S.-H.; Hutmacher, D. Poly(ε-caprolactone) films as a potential substrate for tissue engineering an epidermal equivalent. *Mater. Sci. Eng. C* **2002**, *20*, 71–75. [CrossRef]
14. Catauro, M.; Raucci, M.; De Marco, D.; Ambrosio, L. Release kinetics of ampicillin, characterization and bioactivity of $TiO_2$/PCL hybrid materials synthesized by sol–gel processing. *J. Biomed. Mater. Res. Part A Off. J. Soc. Biomater. Jpn. Soc. Biomater. Aust. Soc. Biomater. Korean Soc. Biomater.* **2006**, *77*, 340–350. [CrossRef] [PubMed]
15. Catauro, M.; Raucci, M.; Continenza, M.; Marotta, A. Biocompatibility tests with fibroblasts of CaO rich calcium silicate glasses. *J. Mater. Sci.* **2004**, *39*, 373–375. [CrossRef]
16. Catauro, M.; Raucci, M.; De Gaetano, F.; Marotta, A. Sol-gel synthesis, characterization and bioactivity of polycaprolactone/$SiO_2$ hybrid material. *J. Mater. Sci.* **2003**, *38*, 3097–3102. [CrossRef]
17. Catauro, M.; Raucci, M.; Ausanio, G. Sol–gel processing of drug delivery zirconia/polycaprolactone hybrid materials. *J. Mater. Sci. Mater. Med.* **2008**, *19*, 531–540. [CrossRef] [PubMed]
18. Rittidach, T.; Tithito, T.; Suntornsaratoon, P.; Charoenphandhu, N.; Thongbunchoo, J.; Krishnamra, N.; Tang, I.M.; Pon-On, W. Effect of zirconia-mullite incorporated biphasic calcium phosphate/biopolymer composite scaffolds for bone tissue engineering. *Biomed. Phys. Eng. Express* **2020**, *6*, 055004. [CrossRef] [PubMed]
19. Soliman, Y.M.; Mabrouk, M.; Abd Raboh, A.S.; Tohamy, K.M.; Beherei, H.H. Influence of the addition of different metal oxides on physicochemical and biological properties of calcium fluorosilicate/PCL bone cement. *J. Mech. Behav. Biomed. Mater.* **2023**, *146*, 106075. [CrossRef]
20. Lacambra-Andreu, X.; Maazouz, A.; Lamnawar, K.; Chenal, J.-M. A review on manufacturing processes of biocomposites based on poly(α-Esters) and bioactive glass fillers for bone regeneration. *Biomimetics* **2023**, *8*, 81. [CrossRef]
21. Kolan, K.; Liu, Y.; Baldridge, J.; Murphy, C.; Semon, J.; Day, D.; Leu, M. Solvent based 3D printing of biopolymer/bioactive glass composite and hydrogel for tissue engineering applications. *Procedia CIRP* **2017**, *65*, 38–43. [CrossRef]
22. De Luna, M.S.; Wang, Y.; Zhai, T.; Verdolotti, L.; Buonocore, G.; Lavorgna, M.; Xia, H. Nanocomposite polymeric materials with 3D graphene-based architectures: From design strategies to tailored properties and potential applications. *Prog. Polym. Sci.* **2019**, *89*, 213–249. [CrossRef]

23. Mashayekhi, S.; Rasoulpoor, S.; Shabani, S.; Esmaeilizadeh, N.; Serati-Nouri, H.; Sheervalilou, R.; Pilehvar-Soltanahmadi, Y. Curcumin-loaded mesoporous silica nanoparticles/nanofiber composites for supporting long-term proliferation and stemness preservation of adipose-derived stem cells. *Int. J. Pharm.* **2020**, *587*, 119656. [CrossRef] [PubMed]
24. Baptista, C.; Azagury, A.; Shin, H.; Baker, C.M.; Ly, E.; Lee, R.; Mathiowitz, E. The effect of temperature and pressure on polycaprolactone morphology. *Polymer* **2020**, *191*, 122227. [CrossRef]
25. Chinaglia, D.L.; Gregorio, R., Jr.; Stefanello, J.C.; Pisani Altafim, R.A.; Wirges, W.; Wang, F.; Gerhard, R. Influence of the solvent evaporation rate on the crystalline phases of solution-cast poly(vinylidene fluoride) films. *J. Appl. Polym. Sci.* **2010**, *116*, 785–791. [CrossRef]
26. Di Maro, M.; Duraccio, D.; Malucelli, G.; Faga, M. High density polyethylene composites containing alumina-toughened zirconia particles: Mechanical and tribological behavior. *Compos. Part B Eng.* **2021**, *217*, 108892. [CrossRef]
27. Castilla-Cortázar, I.; Vidaurre, A.; Marí, B.; Campillo-Fernández, A.J. Morphology, crystallinity, and molecular weight of poly(ε-caprolactone)/graphene oxide hybrids. *Polymers* **2019**, *11*, 1099. [CrossRef] [PubMed]
28. Najafabadi, F.M.; Karbasi, S.; Benisi, S.Z.; Shojaei, S.; Poursamar, S.A.; Azadani, R.N. Evaluation of the effects of alumina nanowire on 3D printed polycaprolactone/magnetic mesoporous bioactive glass scaffold for bone tissue engineering applications. *Mater. Chem. Phys.* **2023**, *303*, 127616. [CrossRef]
29. Mofokeng, J.; Luyt, A. Morphology and thermal degradation studies of melt-mixed poly(lactic acid)(PLA)/poly(ε-caprolactone)(PCL) biodegradable polymer blend nanocomposites with $TiO_2$ as filler. *Polym. Test.* **2015**, *45*, 93–100. [CrossRef]
30. Correlo, V.M.; Boesel, L.F.; Bhattacharya, M.; Mano, J.F.; Neves, N.M.; Reis, R.L. Hydroxyapatite reinforced chitosan and polyester blends for biomedical applications. *Macromol. Mater. Eng.* **2005**, *290*, 1157–1165. [CrossRef]
31. Nunes, R.W.; Martin, J.R.; Johnson, J.F. Influence of molecular weight and molecular weight distribution on mechanical properties of polymers. *Polym. Eng. Sci.* **1982**, *22*, 205–228. [CrossRef]
32. Serra, T.; Planell, J.A.; Navarro, M. High-resolution PLA-based composite scaffolds via 3-D printing technology. *Acta Biomater.* **2013**, *9*, 5521–5530. [CrossRef] [PubMed]
33. Woodruff, M.A.; Hutmacher, D.W. The return of a forgotten polymer—Polycaprolactone in the 21st century. *Prog. Polym. Sci.* **2010**, *35*, 1217–1256. [CrossRef]
34. Peterson, G.I.; Ko, W.; Hwang, Y.-J.; Choi, T.-L. Mechanochemical degradation of amorphous polymers with ball-mill grinding: Influence of the glass transition temperature. *Macromolecules* **2020**, *53*, 7795–7802. [CrossRef]
35. Park, B.; Peterson, G.I. Comparing molecular weight models for polymer degradation with ball-mill grinding. *Polym. Degrad. Stab.* **2023**, *218*, 110549. [CrossRef]
36. Nilagiri Balasubramanian, K.B.; Ramesh, T. Role, effect, and influences of micro and nano-fillers on various properties of polymer matrix composites for microelectronics: A review. *Polym. Adv. Technol.* **2018**, *29*, 1568–1585. [CrossRef]
37. Rahaman, M.; Aldalbahi, A.; Bhagabati, P. Preparation/processing of polymer–carbon composites by different techniques. In *Carbon-Containing Polymer Composites*; Springer: Singapore, 2019; pp. 99–124.